Journal of the Argentine Chemical Society

EVALUATION OF CRYSTAL FIELD EFFECTS OF Yb^{3+} IN MONOCLINIC $KGd(WO_4)_2$ AND $KYb(WO_4)_2$ LASER CRYSTALS. COMPARISON WITH DISORDERED TETRAGONAL $NaGd(WO_4)_2$ CRYSTALS

C. Cascales

Instituto de Ciencia de Materiales de Madrid, Consejo Superior de Investigaciones Científicas.

C/ Sor Juana Inés de la Cruz, 3. Cantoblanco, 28040 Madrid, Spain.

E-mail: *ccascales@icmm.csic.es*. **Fax**: +34 913720623

Received August 11, 2008. In final form February 15, 2009.

Abstract

The knowledge of the crystal field potential imposed by a given host is crucial to determine the laser performances of the corresponding Yb^{3+} and Tm^{3+} doped crystals. Methods to reproduce the crystal field effects of Yb^{3+} in monoclinic $KGd(WO_4)_2$ and $KYb(WO_4)_2$, and in tetragonal $NaGd(WO_4)_2$ double tungstate laser crystals, provide the assessment to interpret the observed low temperature spectra, and confidently establish their energy level sequences, especially when the symmetry of the optically active point site is quite low. Furthermore, crystal field strengths in combination with the spectral features observed in low temperature spectra, manifold splittings and broadening bandwidth values, allow rationalizing the prediction of the specific kind of laser potential in both families of double tungstates.

Keywords: crystal field; laser crystals; double tungstates.

Resumen

El conocimiento del potencial del campo del cristal creado por una matriz dada es de importancia crucial en la determinación del funcionamiento como láseres de los cristales dopados con Tm^{3+} e Yb^{3+}. Los métodos capaces de reproducir los efectos del campo del cristal para Yb^{3+}, tanto en los cristales láser dobles volframatos monoclínicos de composición $KGd(WO_4)_2$ y $KYb(WO_4)_2$, como en los de estructura tetragonal $NaGd(WO_4)_2$, proporcionan herramientas para la interpretación de los espectros ópticos de baja temperatura, y establecer de forma segura las correspondientes secuencias de niveles de energía, en especial cuando la simetría del sitio puntual ocupado en la red es muy baja. La combinación de los parámetros de fuerza del campo del cristal con las características que muestran los espectros ópticos –desdoblamientos múltiples y aumentos en los anchos de las bandas espectrales–, permite además racionalizar la predicción del tipo de potencial láser que cabe esperar de ambas familias de dobles volframatos.
Palabras clave: campo del cristal, cristales láser, dobles volframatos.

Introduction

The interest in double tungstate $MT(WO_4)_2$ crystals (shortly MTW) derived from the substitution of Ca^{2+} in the tetragonal scheelite-type $CaWO_4$ by a couple of M^+ and T^{3+} cations, M = alkali cation or Ag, T = rare-earth RE (RE=Y, La or lanthanide), In, or Bi, started on with the early demonstrations of stimulated emission of Nd^{3+} in simple XWO_4 (X=Ca^{2+}, Sr^{2+} or Pb^{2+}) [1,2] as well as in double $Na_{0.5}Gd_{0.5-x}Nd_xWO_4$ tungstates [3]. Subsequent extensive studies on their phase diagrams, crystal growth and crystallographic characteristics performed in Russian labs [4,5] revealed that the polymorphism is a distinctive feature of MTW compounds, and in fact, depending on the M-T ionic radii relationship and on the temperature of the synthesis (or crystal growth) different phases have been found, including the tetragonal scheelite-type of the $CaWO_4$ (space group $I4_1/a$ (No. 88)), but also orthorhombic, monoclinic or even triclinic symmetries. Later on research activities on MTW focused in the relationship between vibronic IR and Raman properties and the crystal symmetry [6,7,8], their scintillating characteristics [9,10], nonlinear optical properties, such as Raman shifting [11] and up-conversion [12], and detailed spectroscopic and crystal field CF analyses of optically active RE^{3+} in several monoclinic KTW (space group $C2/c$ (No. 15)) [13,14,15,16] and tetragonal NaBiW (space group $I\bar{4}$ (No. 82)) [17,18,19,20,21] hosts. But it was not until more recently, mainly with the development of the pumping technology using high-power semiconductor diode lasers DL, that ultimate capabilities of these crystals as laser and nonlinear materials as well as for optical cooling have been completely revealed. This initially concerned the strongly anisotropic (biaxial) monoclinic KYW, KGdW and KLuW crystals [22]. Such crystals, characterized by the possibility of being doped with high concentrations of the optically active RE^{3+} ions without substantial fluorescence quenching as well as high values of the absorption and emission cross sections of these dopants, have found applications in continuous wave (cw) and pulsed high-power laser systems, and as solid-state stimulated Raman laser shifters [11]. Crystals doped with Yb^{3+} [23,24,25] and Tm^{3+} [26] have lately concentrated the interest as these cations possess optical absorption bands that can be pumped by InGaAs and AlGaAs DL, respectively.

In contrast to the potassium-based double tungstates, MTW crystals with M=Li or Na and T = Y, La, Gd, Lu or Bi, possessing tetragonal $I\bar{4}$ crystallographic structure present local disorder associated to the random distribution of M^+ and T^{3+} cations on the same lattice sites [27]. When doped with optically active RE^{3+} cations their optical absorption and photoluminescence spectra show substantial inhomogeneous broadening, and although with proportional decrease in peak absorption and emission cross-sections with regard to KTW counterparts, enlarged gain bandwidths

allow very efficient high power diode-pumping, and the achievement of extended Yb^{3+} [28] and Tm^{3+} [29] laser tunability and ultrashort pulse generation [28,30,31].

The main disadvantage of Tm^{3+} and Yb^{3+} as quasi-three level laser systems for ~1.95 μm ($^3F_4 \rightarrow {}^3H_6$) and ~1 μm ($^2F_{5/2} \rightarrow {}^2F_{7/2}$) spectral ranges, respectively, is the thermal population of the terminal level, which belongs in both cases to the ground state multiplet. Consequently, the critical dependence of the laser performance on host properties, such as crystal field strength and ion-host interactions, imposes the need for a reliable determination of the involved Stark levels in order to calculate the partition functions used in the evaluation of the emission and gain cross sections for the indicated Tm^{3+} and Yb^{3+} laser transitions. However, the unambiguous identification of energy levels in these $4f^{12}$ and $4f^{13}$ configurations is usually problematic, mainly due to the strong interaction with lattice vibrations [32], and for the first one is specially complicated given the scarce number of energy levels, which prevent the phenomenological determination of crystal field effects and Stark levels [33,34].

The current paper proposes an approach to the determination of the parameters describing the CF potential of Yb^{3+} in the C_2 site symmetry of the monoclinic KGdW as well as in the stoichiometric KYbW laser crystals, which will allow to discuss the previously proposed sequences of energy levels [35,36,37,38]. As an assessment in this study, trends of CF effects through the series of optically active RE^{3+}=Pr [14], Nd [13], Ho, Er [15] and Tm [16] doping the KGdW host will be examined. Comparisons between low temperature optical absorption spectra related to the 1 μm and 1.95 μm laser emissions of Yb^{3+} and Tm^{3+}, respectively, will underline differences associated with the local ordered and disordered character in both monoclinic KGdW and tetragonal NaGdW laser crystals.

Crystallographic background

KTW crystals belong to the monoclinic system, with space group *C*2/*c* (No. 15), and unit cell parameters *a*=10.652(4)/10.590(4) Å, *b*=10.374(6)/10.290(6) Å *c*=7.582(2)/7.478(2) Å and β=130.80(2)º/130.70(2) for KGdW [39] /KYbW [40]. The structure is constituted by double chains of edge-sharing WO_6 distorted octahedra running along the *c* direction, chains of KO_{12} distorted icosahedra along [$\bar{1}$10], and Gd^{3+} cations, which occupy only one crystal site, are coordinated to eight oxygens forming GdO_8 distorted square antiprisms, with four different Gd-O distances, in single chains extended along the [110] direction. The local symmetry of Gd^{3+} (as well as optically active RE^{3+} cations replacing Gd^{3+}) in its first coordination sphere only contains a C_2 axis parallel to the *b* axis of the lattice. The Figure 1a shows a view of this structure in the *ac* plane.

NaTW crystals belong to the non-centrosymetric tetragonal space group $I\bar{4}$ (No. 82) [28,41], with Na^+ and T^{3+} (and RE^{3+}) sharing two different crystal sites, 2*b* and 2*d*, both with S_4 point symmetry. Figure 1b shows a view of this tetragonal structure, which contains two kinds of WO_4 tetrahedra and Na/TO_8 square antiprisms. Along *a* and *b* directions the structure is built of parallel chains of alternate, sharing-edge Na/TO_8 and WO_4 polyhedra, of only one type in each row, and in the *c* direction Na/TO_8 polyhedra from two different consecutive chains are linked through a common edge, forming $(Na/T)_2O_{14}$ dimeric units. Although T^{3+} has 8-fold oxygen coordination in both sites, T-O distances and O-T-O angles are different for each site. Furthermore, multiple short-range Na^+ and T^{3+} environments (namely "local disorder") in the first cationic shell around each optically active RE^{3+} replacing T^{3+} generate a distribution of crystal fields. Since the magnitude of the spectral bandwidth is determined by a convolution of the lineshapes from the local environments around the different point sites, the existence of two crystallographic sites for the optically active lanthanide in $I\bar{4}$ enhances the spectral broadening, and consequently the related laser tunability.

Besides the "order" and "local disorder" that characterize KTW and NaTW structures, there is another difference between these crystals. While both S_4 Na/TO_8 square antiprisms are highly regular polyhedra, the C_2 GdO_8 polyhedron is characterized by a distribution of Gd-O distances among which one is clearly shorter than the average value.

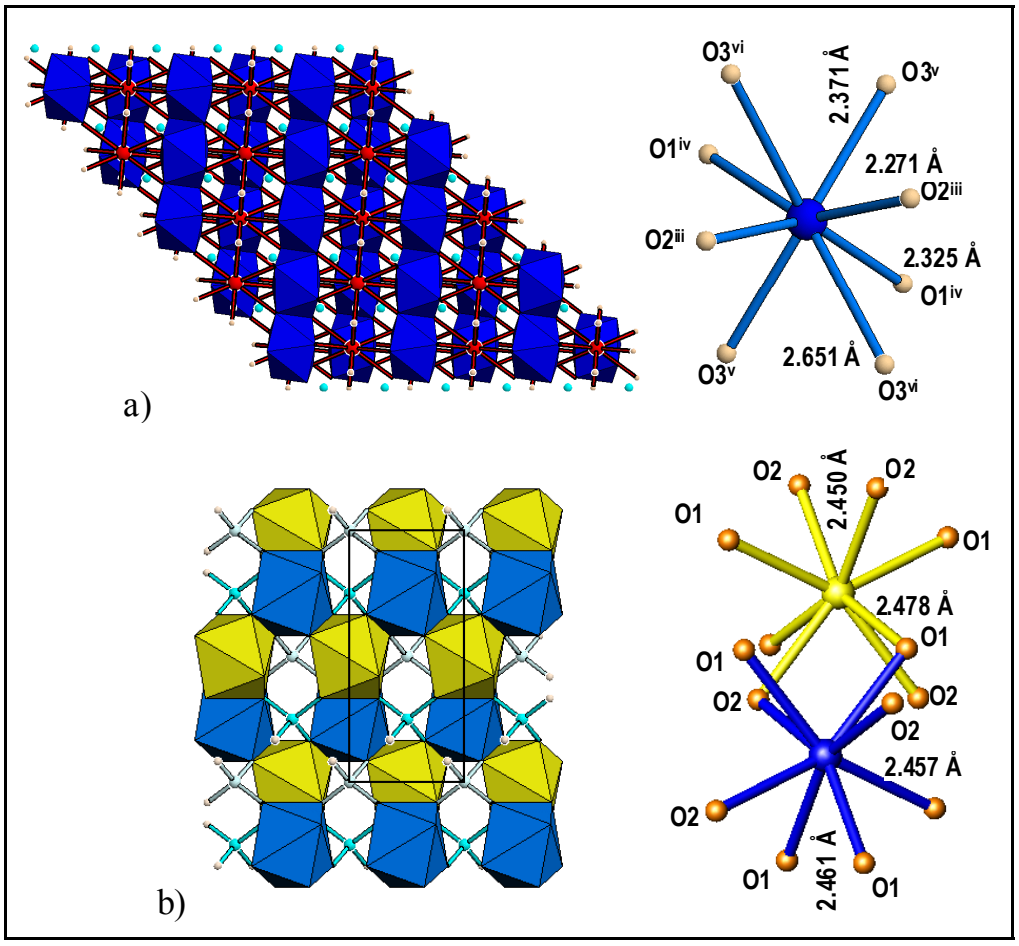

Figure 1. a) View in the *ac* plane of the monoclinic *C*2/*c* structure of $KT(WO_4)_2$ showing the TO_8 chains along the [101] direction (left), and the TO_8 coordination polyhedron with C_2 symmetry (right); b) View in the *ac* plane of the tetragonal $I\bar{4}$ structure of $NaT(WO_4)_2$, with WO_4 tetrahedra connecting dimeric units $(Na/T)_2O_{14}$ along the *c* direction, light (online yellow) and dark (online blue) polyhedra correspond to (Na/T) cations in 2*b* and 2*d* lattice sites, respectively (left), and the two $(Na/T)O_8$ polyhedra, both with S_4 symmetry (right).

Low temperature spectroscopic properties of Yb^{3+} in $KGd(WO_4)_2$ and in $KYb(WO_4)_2$ crystals: Yb^{3+} energy level splittings.

The C_2 symmetry for the Yb^{3+} site in the monoclinic KGdW host splits the two multiplets $^2F_{7/2}$ (n) and $^2F_{5/2}$ (n') into four (n = 0, 1, 2, 3), and three (n' = 0', 1', 2') double degenerate Stark levels, respectively. For this symmetry polarization dependent selection rules for the electronic transitions of the $4f^{13}$ configuration are not expected. This means that the number and the positions of the absorption peaks have to be independent of the polarization but intensity variation of the peaks associated with the three polarizations is still possible. In fact, a strong anisotropy for this biaxial crystal has been confirmed experimentally, both in the spectra recorded at room temperature and at lower temperatures [35,36,37].

Figure 2a shows the unpolarized 6 K optical absorption spectrum corresponding to $^2F_{7/2}$ (0) → $^2F_{5/2}$ (n'= 0', 1', 2') transitions (shortly 0 → n') of Yb^{3+} (1.0 mol %) in KGdW. A single and very sharp band is observed at 10196 cm^{-1}, which is ascribed to the 0→0' Yb^{3+} transition, in agreement with the existence of a single 4*e* site for Yb^{3+} ions in the KGdW crystal structure. The linewidth of this transition (as full-width at half maximum FWHM) is 3.7 cm^{-1}. For comparison, the FWHM of the same transition in the disordered tetragonal Yb^{3+} in NaGdW, Figure 2b, is four times larger, ~15 cm^{-1} [28,42]. The broadening is attributed to the distribution of slightly different crystal fields around Yb^{3+} centers due to the local cationic disorder created by the Yb^{3+} substitution over the two shared 2*b* and 2*d* crystal sites [27,28,30,31,42]. A second set of overlapped bands is observed in the OA spectrum of Yb^{3+} in KGdW between 10420 and 10515 cm^{-1}, making difficult to ascertain accurately the energy that corresponds to the 0→1' transition. Finally, another OA set of bands appears in the 10580-10750 cm^{-1} region, and once again the assignment of the 0→2' Yb^{3+} transitions is not clear. Despite its simplicity, the proclivity of the $4f^{13}$ electronic structure of Yb^{3+} to interact with lattice vibrations [32], which can give rise to intense vibronic sidebands and additional effects as shifting or splitting of lines in case of resonant coupling, usually complicates the identification of some of its energy levels. In this way, strong phonon-electron couplings have been claimed in Yb^{3+}-doped KGdW and in stoichiometric KYbW [38] monoclinic crystals to explain the complex low temperature OA spectra. From the 6 K OA spectrum of Yb^{3+} in KGdW, Figure 2a, the observed bands appear at (cm^{-1}) 10196, 10460, 10490, 10598, 10614, 10631, 10687 and 10728 [37], i.e., eight bands instead of the three expected ones. Previous studies have established the sequence of $^2F_{5/2}$ energy levels of Yb^{3+} in KGdW as (cm^{-1}) 10188, 10471 and 10682 [35] (therein $^2F_{5/2}$ Stark levels of Yb-KGdW scheme 1), and as 10196, 10491 and 10686 ($^2F_{5/2}$ Yb-KGdW scheme 2) [36]. On the other hand, when the stoichiometric KybW crystal is considered, the energies of these Stark levels have been determined as (cm^{-1}) 10188, 10500 and 10734 [38].

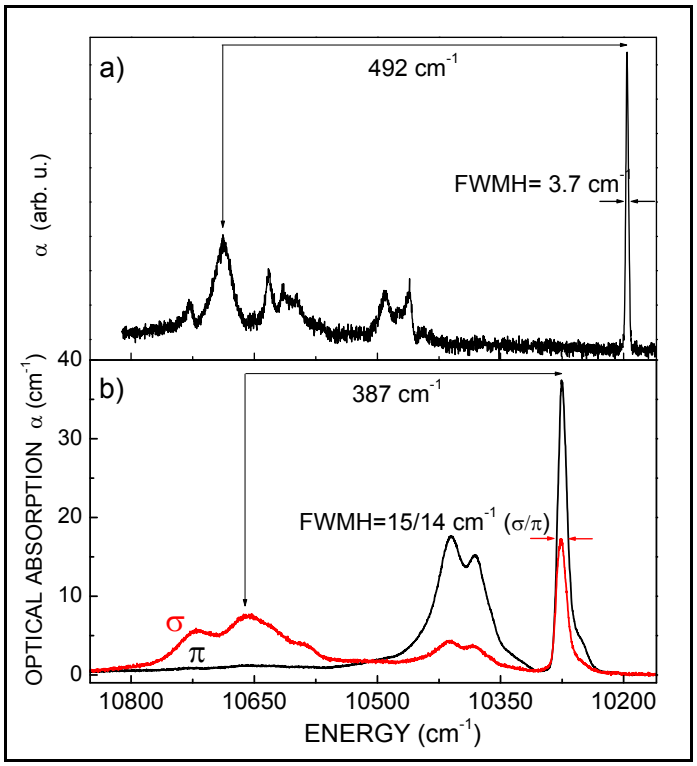

Figure 2. 6 K optical absorption spectra of a) 1.0 mol % Yb-doped $KGd(WO_4)_2$ and b) 0.1 mol % Yb-doped $NaGd(WO_4)_2$. Comparison of splittings of the excited $^2F_{5/2}$ Yb^{3+} multiplet and bandwidths of the $^7F_{7/2}(0)\rightarrow{}^7F_{5/2}(0')$ transition.

The low temperature photoluminescence PL spectrum of Yb^{3+} must display four bands associated to $^2F_{5/2}$ (0') → $^2F_{7/2}$ (n = 0, 1, 2, 3) (shortly 0' → 0, 1, 2, 3) transitions. In addition to reabsorption effects [33,34,38] PL bands also appear combined with some superimposed vibronic structure. From the analysis of the 6 K PL spectrum of Yb^{3+} in KGdW $^2F_{7/2}$ Stark energy levels at (cm^{-1}) 0, 163, 385 and 535 [35] (therein $^2F_{7/2}$ Yb-KGdW schemes 1 and 2) have been established. The study for the stoichiometric KybW [38], which includes comparisons with Raman modes, indicates this sequence as (cm^{-1}) 0, 168, 438 and 555.

Crystal field modelling, crystal field strengths and simulation of crystal field energy levels.

Considering the limits imposed by the special features of the $4f^{13}$ configuration of Yb^{3+} -only seven Stark levels from which we can not unequivocally derive a phenomenological CF potential description, specially for the current C_2 symmetry involving up to 14 B_q^k CF parameters, and the difficulty for deriving the energy level diagram from the low-temperature OA and PL spectra, some predictive tools must used to determine these data for Yb^{3+} in KGdW and in KYbW laser hosts.

Initially the proposed distributions of Yb^{3+} energy levels have been checked using the so-called 'barycenters plot' method [43] This method considers that the energy separation between the ground $^2F_{7/2}$ and excited $^2F_{5/2}$ multiplets is constant, independently of the matrix, and equal to the spin-orbit splitting for the free-ion, and therefore the energies of both $^2F_{7/2}$ and $^2F_{5/2}$ barycenters present a linear relationship, see the Figure 3a, where data for several laser hosts have been represented [43]. Thus, barycenters at 271 and 10447 cm^{-1}, for proposed scheme 1 [35], and at 271 and 10458 cm^{-1}, for scheme 2 [36] of Yb-KGdW, and at 290 and 10474 cm^{-1} for the stoichiometric KYbW, have been now included in the Figure 3a, and for clarity Figure 3b shows an enlarged view of this area, which also contains the corresponding data for tetragonal disordered Yb-NaTW, T=Y^{3+} [31], Gd^{3+} [28] and Lu^{3+} [30] counterparts.

From currently plotted data in Figure 3b it can be observed a better fit with the constant energy-separation line for Yb^{3+} Stark levels of scheme 1 than for these of scheme 2. Also, a certain misalignment is observed for barycentres of KYbW. On the other hand, it seems that previously established Stark levels for an average optical center in tetragonal NaTW crystals adequately satisfy the "barycenters law", confirming energy level assignments. When barycenters for both kinds of crystal phases are compared, the higher ones correspond with no doubt to monoclinic KYbW and to Yb-KYW [35], however these of Yb-KGdW are closer to results for Yb-NaTW crystals.

After this test, the first approach to the CF modelling considers the use of some semi-empirical calculation model for CF interactions. We applied the well-tested Simple Overlap Model SOM [44], which calculates CF parameters from previous structural data of the compound [39]. SOM considers effective charges, located around the middle of the Yb^{3+}-oxygen distances, which are assumed to be proportional to the magnitude of the overlap integral, ρ, between the Yb^{3+} and oxygen wavefunctions. Results of simulated C_2 SOM CF parameters are included in Table 1. Then, the calculation of the sequence of energy levels requires only two free-ion parameters, E_0 and the spin-orbit coupling constant ζ, whose variation with the crystal host is theoretically predicted to be weak for a given RE^{3+} ion, and consequently can be reasonably taken from the literature [45].

A more phenomenological method consists on the evaluation of trends in the variation of CF parameters for several RE^{3+} doping ions in the same KGdW host, followed for the extrapolation to Yb^{3+}. C_2 crystal field parameters for RE^{3+}= Pr^{3+} [14], Nd^{3+} [13], Ho^{3+}, Er^{3+} [15], and Tm^{3+} [16] are available, and can be used for this purpose. However, in several RE-containing families it has been observed that besides normal fluctuations of these parameters, some discontinuity in variation trends is observed towards the middle of the series, Eu^{3+}-Tb^{3+} [46], and from this point of view, parameters derived from the CF analysis of the low temperature Er^{3+}, and specially Tm^{3+}-optical spectra will constitute the best guide to the confirmation of Yb^{3+} energy levels. Since a true

adjustment is not possible for Yb^{3+}, to simulate the experimentally proposed $^2F_{5/2}$ and $^2F_{7/2}$ manifolds we examine the energy level sequences resulting of small modifications in CF parameters according their evolution from Er^{3+} and Tm^{3+} (the five complex S^k_q are kept as for Tm^{3+} in KGdW), and only the two required free ion parameters, E^0 and ζ, will be allow to freely change. These calculations have been carried with the program IMAGE [47]. Optimized sets of CF parameters that better reproduce Yb^{3+} energy level schemes 1 and 2 appear in Table 1.

With the same $^2F_{7/2}$ energy levels, experimentally proposed schemes 1 and 2 for Yb-KGdW crystal have similar $^2F_{5/2}$ total splittings, 494 and 492 cm^{-1}, respectively. However, the distribution of Stark levels within the excited multiplet is quite different, yielding a higher barycenter for the later sequence. Taking into account results in Figure 3, i.e., the better alignment of barycenters for scheme 1, it can be though that the energy position of $^2F_{5/2}$ (1') is overestimated in scheme 2. Accordingly, the peak that corresponds to the ground absorption to $^2F_{5/2}$ (1') in the 10420-10515 cm^{-1} region of the low temperature OA spectrum for Yb-KGdW shown in Figure 2 must be this appearing at the lower energy side of the band, 10460 cm^{-1}, instead of the considered at 10491 cm^{-1}.

Concerning the experimental sequence of energy levels proposed for KYbW [38], with splittings for $^2F_{7/2}$ and $^2F_{5/2}$ that should be closer to corresponding values for Yb^{3+} in KYW, its is reasonable to think that its $^2F_{5/2}$ barycenter must lie at lower energy than the indicated in Figure 3b. From this point of view the peak near 10710 cm^{-1} in Figure 7 of [38] seems to be a better choice for the low temperature ground OA to $^2F_{5/2}$(2') than the indicated at 10734 cm^{-1}.

When for a given crystalline host the number of CF parameters is large, as in the current case, the knowledge of the relative S^k (k = 2, 4, 6) and total S^T CF strength parameters [48] is a useful tool to establish quantitative comparisons of the CF potential across the $4f^N$ series. S^2, S^4 and S^6 are rotational invariants of the crystal field (see the corresponding definitions at the bottom of Table 2 [48]), which represent the short-, mid- and long-range CF strengths, respectively, in connection with the spatial expansion of CF effects. Given the high number of four- and six-rank parameters involved in the CF potential at the RE^{3+} crystal site in the monoclinic KTW structure, trends in medium- and long-range CF effects must be summarized through corresponding S^4 and S^6 strengths.

CF strength parameters as a function of the number of *f* electrons in KGdW are plotted in Figure 4, and for RE^{3+}= Tm^{3+} [16] and Yb^{3+} their numerical values are also included in Table 2. For a same host the CF effect would be expected to weaken over the $4f^N$ series with the increased nuclear charge to which the electrons are subjected from Pr^{3+} to Yb^{3+}, since the electron orbitals are pulled closer to the nucleus. For the KGdW host, using results from current as well as previous CF analyses [13,14,15,16], it is clear that S^4 and S^6 evolve with negative slopes from Pr^{3+} to Yb^{3+}, see the Figure 4, trend also negative for S^2 from Ho^{3+} to Yb^{3+}. The overall CF strength, S^T, which accounts for all CF parameters and describes the total CF strength, shows a decreasing evolution along all the $4f^N$ series. Discontinuities in the evolution of individual CF parameters, i.e., some observed inflection points in the general behavior, are similar to these observed in extensively studied RE^{3+}-doped crystal hosts [33,34,45].

Figure 4 also includes S^k and S^T data for Yb^{3+} in the stoichiometric KYbW crystal. Now S^2 and S^4 and S^T regain strength with regards to the doped KGdW crystal, although the two latter parameters hold up the decreasing trend from the middle of the series. These results are not surprising since these parameters are especially sensitive to modifications in the close coordination shell of the optically active RE^{3+} ion, and it is likely that the CF weakening due to the nuclear charge increase criterion is compensated, and for S^2 even surpassed, by an enhancement derived of the shortening of some Yb-O distance in YbO_8 of KYbW with regards to GdO_8 in KGdW [39.40]. Furthermore, differences between sets of CF strength parameters for Yb^{3+} in KGdW and in KYbW crystals are reflecting specific crystallographic features of the C_2 sites that they are occupying. Larger values of S^2 and S^4 for KYbW suggest a more ionic and distorted Yb^{3+} short–range

environment than in KGdW. This fact agrees with the larger distribution of Yb-O distances [in the 2.198(7)- 2.711(6) Å range], along with the shorter average Yb-O distance $\bar{d}_{Yb-O}$ = 2.362(8) Å [40], in the coordination polyhedron YbO_8 with regards to these in GdO_8 [2.271(12)- 2.650(11) Å, and $\bar{d}_{Gd-O}$ = 2.404(12) Å] [39]. RE^{3+} local environments can also be numerically featured by the calculated distortion degree $\Delta_d \times 10^3$ of the corresponding REO_8 polyhedron [49], 7.6 and 3.7 for RE^{3+} = Yb and Gd, respectively. However, the trend is not maintained for long-range S^6 parameters. It can be explained through the expected more compact and covalent WO_6 octahedral arrangement around Yb^{3+} sites in the stoichiometric crystal than in Yb-doped KGdW.

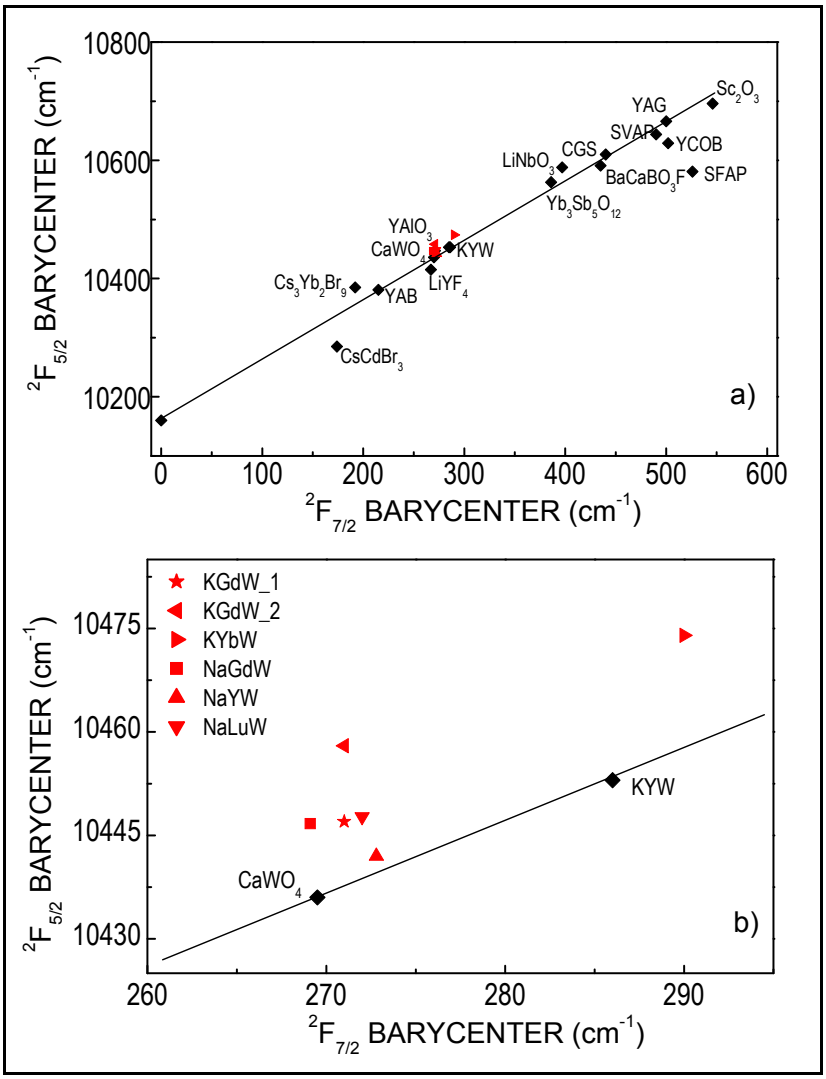

Figure 3. a) Plot of the barycenters for several Yb-doped laser crystals, and b) enlargement of the plot for ordered monoclinic $KT(WO_4)_2$ and disordered tetragonal $NaT(WO_4)_2$ laser crystals.

Table 1. Free-ion and optimized C_2 crystal field CF parameters (B_q^k,S_q^k) used to calculate the $^2F_{7/2}$(n) and $^2F_{5/2}$(n´) energy levels of Yb^{3+} in $KGd(WO_4)_2$ and $KYb(WO_4)_2$ laser crystals. Italics indicate CF parameters calculated from SOM [44] (ρ = 0.07, effective charge for oxygen = -1). The experimentally determined energy levels are below in italics. Parameters and energies are given in cm^{-1}. Values in parentheses refer to estimate standard deviations in the indicated parameter. Values in square brackets were not varied in the reproduction of the Yb^{3+} energy level sequences. For comparison, phenomenological CF parameters for closer $4f^{11}$ (Er^{3+}) and $4f^{12}$ (Tm^{3+}) configurations in $KGd(WO_4)_2$ have been also included.

	SOM	**Yb-KGdW-1**	**Yb-KGdW-2**	**KYbW**	**Er-KGdW**	**Tm-KGdW**
E^0		4632(3)	4637(3)	4652(3)		
ζ		2906(2)	2909(2)	2906(2)		
B_0^2	*433*	320	335	290	303(28)	299(16)
B_2^2	*267*	335	345	410	260(33)	363(11)
B_0^4	*-752*	-960	-930	-1060	-986(47)	-893(26)
B_2^4	*258*	-60	-30	-30	25(63)	36(26)
S_2^4	*-708*	[-676]	[-676]	[-676]	-811(30)	-676(19)
B_4^4	*-163*	175	185	170	250(53)	-36(28)
S_4^4	*237*	[276]	[276]	[276]	381(38)	276(29)
B_0^6	*-191*	-20	-20	5	36(67)	-27(39)
B_2^6	*186*	230	233	190	173(51)	231(32)
S_2^6	*98*	[48]	[48]	[48]	229(38)	48(30)
B_4^6	*72*	25	25	10	5(63)	-139(28)
S_4^6	*21*	[119]	[119]	[119]	-14(62)	119(28)
B_6^6	*-153*	-50	-50	-75	-173(42)	-34(37)
S_6^6	*141*	[176]	[176]	[176]	125(44)	176(28)
$^2F_{5/2}$ (2')		10672 *10682*	10682 *10688*	10704 *10734*		
$^2F_{5/2}$ (1')		10467 *10471*	10484 *10491*	10499 *10500*		
$^2F_{5/2}$ (0')		10202 *10188*	10209 *10196*	10200 *10188*		
$^2F_{7/2}$ (3)		540 *535*	540 *535*	563 *555*		
$^2F_{7/2}$ (2)		389 *385*	392 *385*	440 *438*		
$^2F_{7/2}$ (1)		156 *163*	160 *163*	163 *168*		
$^2F_{7/2}$ (0)		0 *0*	0 *0*	0 *0*		

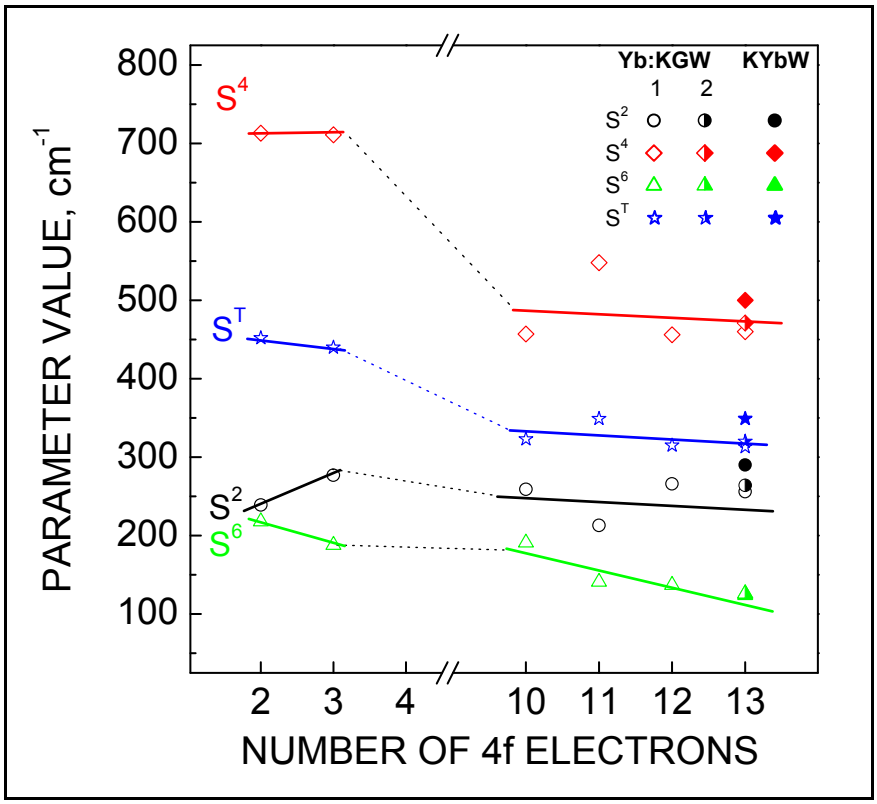

Figure 4. Evolution of crystal field strength parameters for $4f^N$ configurations in $KGd(WO_4)_2$ crystals. For $4f^{13}$ configuration empty symbols refer to Yb^{3+} energy levels of scheme 1 [35], medium-filled symbols for energy levels of scheme 2, and full symbols for Yb^{3+} in $KYb(WO_4)_2$.

Crystal field strength and low temperature spectral broadening in monoclinic $KGd(WO_4)_2$ and tetragonal $NaGd(WO_4)_2$ laser crystals: Discussion of some differences in laser performance.

Along with the exploration of the evolution of the CF potential *across* one same structural family of doped materials, the analysis of S^k and S^T values will allow establish comparisons *inter* different hosts, even if the point symmetry of the active site is not the same and different sets of CF parameters are involved in its description. Table 2 contains the values of S^k and S^T parameters for Tm^{3+} and Yb^{3+} laser ions in both monoclinic and tetragonal double tungstates [50,28].

In contrast to KGdW, only S^4 experiences some weakening going from Tm^{3+} to Yb^{3+} in NaGdW crystals, and S^2 is now stronger for the later configuration, an indication of the more distorted local surroundings of Yb^{3+} sites. But being the total CF potential quite similar in both KGdW and NaGdW hosts, an important difference found is the considerably higher short-range CF strength in the ordered monoclinic KGdW structure. This fact is related to the observed larger CF splittings for several multiplets in KGdW with respect to NaGdW counterparts, as can be observed in Figure 2 and Figure 5 for selected OA transitions of Yb^{3+} and Tm^{3+} crystals, respectively, and supposes an important benefit for efficient lasing as $^2F_{7/2}$ and $^3H_6$ ground states must be larger as possible to overcome high pumping intensity thresholds usual in these quasi-three level laser systems. Thin-disk configurations of these K crystals have great potential in power-scaling [51].

Other relevant difference in low temperature optical spectra of the studied double tungstates is the four times larger bandwidths of the disordered tetragonal phase. In this case, since both the $^3H_6 \rightarrow {}^3H_4$ transition of Tm^{3+}, and the $^2F_{7/2} \rightarrow {}^2F_{5/2}$ of Yb^{3+} can absorb the ~800 nm and ~ 980 nm emissions of AlGaAs and InGaAs DL, respectively, the efficiency in their resonant pumping will be enhanced by tetragonal disordered hosts providing broader bandwidths, which relax the requirements to the pump source and reduce the sensitivity to thermal drifts of the pump wavelength. Broader emission lines are, on the other hand, very advantageous for tunable and mode-locked ultrashort laser pulsed operation [28,29,30,31,50,52,53].

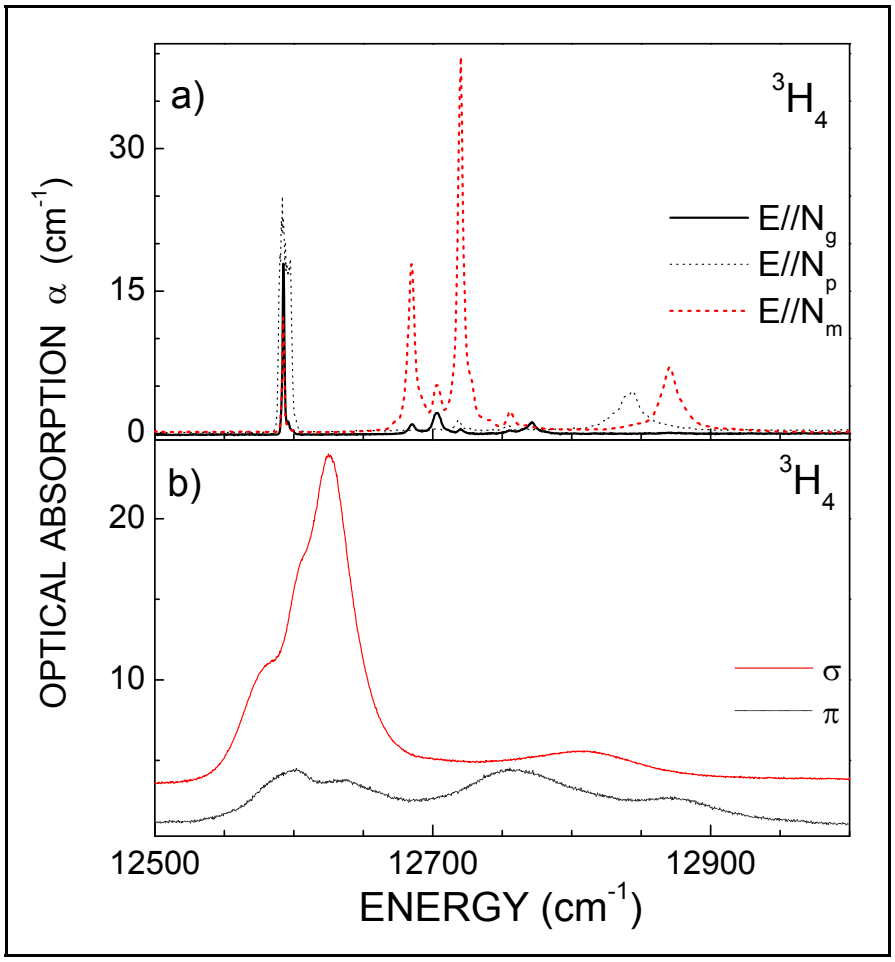

Figure 5. Comparison of the 6 K polarized optical absorption spectra for the $^3H_6 \rightarrow {}^3H_4$ for a) monoclinic Tm-$KGd(WO_4)_2$, and b) tetragonal Tm-$NaGd(WO_4)_2$ laser crystals. According to the crystallographic model of the tetragonal $NaGd(WO_4)_2$ host, both optical Tm^{3+} centers have S_4 inversion axes parallel to the *c* crystal axis, and, thus, experimental spectra have been labeled σ ($E \perp c$; $B \parallel c$) or π ($E \parallel c$; $B \perp c$). For the monoclinic $KGd(WO_4)_2$ host the principal axis of the optical indicatrix with lowest refractive index is labelled *p* and is parallel to the crystallographic *b* axis. The principal axis with the highest refractive index is labelled *g* and is in the *ac* plane forming with the *c* axis an angle ~20 º in the clockwise direction when looking from the positive end of the *b* axis. Finally, the principal axis with intermediate refractive index is labeled *m* and is in the *ac* plane orthogonal with the *g* principal axis, and thus experimental spectra have been taken with light polarized along these directions.

Table 2. Crystal field strength parameters S^k (k = 2, 4, 6) and S^T (see definitions at the bottom) (cm^{-1}) for Tm^{3+} and Yb^{3+} in monoclinic $KGd(WO_4)_2$ and tetragonal $NaGd(WO_4)_2$ laser crystals.

	Tm^{3+}			Yb^{3+}	
	KGdW	**NaGdW**		**KGdW**	**NaGdW**
S^2	266	152		256	209
S^4	456	435		460	412
S^6	137	211		126	222
S^T	315	293		313	296

$$S^k = \left\{ 1/(2k+1) \left[(B_0^k)^2 + 2\sum_q \left[(B_q^k)^2 + (S_q^k)^2 \right] \right] \right\}^{1/2}$$

$$S^T = \left[\frac{1}{3} \sum_k S_k^2 \right]^{1/2}$$

Conclusions

Predictive methods to reproduce the crystal field effects of Yb^{3+} in monoclinic KGdW and KYbW, and in tetragonal NaGdW double tungstate laser crystals provide the assessment to interpret the observed low temperature spectra and confidently establish their energy level sequences, especially when the symmetry of the optically active point site is quite low. Furthermore, crystal field strength parameters combined with the spectral features observed in low temperature spectra allow to rationalize the prediction of laser performances in both kinds of double tungstates.

Acknowledgments. This work is supported by the Spanish Project MAT2008-06720-C02-01.

References

[1] L.F. Johnson, R. R. Soden. *J. Appl. Phys*. **1962**, *33*, 757.

[2] L.F. Johnson, G. D. Boyd, K. Nassau, R. R. Soden. *Phys. Rev*. **1962**, *126,* 1406.

[3] G. E. Peterson, P. M. Bridenbaugh. *Appl. Phys. Lett*. **1964***, 4,* 173.

[4] M.V. Mokhosoev, F.P. Alexeev, and V.I. Lutsyk, *Phase Diagrams of Molybdate and Tungstate Systems* (Nauka, 1978, 320 p) (in Russian).

[5] V.K. Tzunov, V.A. Efremov, Yu.A. Velihkodnyi, *Crystallochemistry and properties of double molybdates and tungstates,* Nauka, Leningrad, 1986 (in Russian).

[6] J. Hanuza, M. Maczka, J.H. van der Maas. *J. Mol. Struct*. **1995**, *348*, 349.

[7] J. Hanuza, A. Benzar, A. Haznar, M. Maczka, A. Pietraszko. J.H. van der Maas, *Vibr. Spectr*. **1996**, *12*, 25.

[8] J. Hanuza, A. Haznar, M. Maczka, A. Pietraszko, A. Lemiec, J.H. van der Maas, E.T.G. Lutz. *J. Raman Spectrosc.* **1997**, *28*, 953.

[9] K. Nitsch, M. Nikl, C. Barta, D. Schultze, A. Triska and R. Uecker, *Phys. Status Solidi A,* **1990**, *118*, K133.

[10] V. G. Baryshevsky, M. V. Korzhik, V. I. Moroz, V. B. Pavlenko, A. S. Lobko, A. A. Fyodorov, V. A. Kachanov, V. L. Solovjanov, B. I. Zadneprovsky, V. A. Nefyodov, P. V. Nefyodov, B. A. Dorogovin and L. L. Nagornaja, *Nucl. Instr. Meth. Phys. Res.* A, **1992**, *322,* 231.

[11] A. A. Kaminskii, S. N. Bagayev, K. Ueda, H. Nishioka, Y. Kubota, X. Chen and A. Kholov, *Jpn. J. Appl. Phys*. **1995**, *34*, L1461.

[12] M. Rico, V. Volkov and C. Zaldo, *J. Alloys Comp*. **2001**, *323-324*, 806.

[13] V. S. Mironov and L. E. Li, *J. Alloys Comp.* **1998***, 279*, 83.

[14] C. Zaldo, M. Rico, C. Cascales, M.C. Pujol, J. Massons, M. Aguiló, F. Díaz and P. Porcher *J. Phys.: Condens. Matter* **2000,** *12*, 8531.

[15] M.C. Pujol, C. Cascales, M. Rico, J. Massons, F. Díaz, P. Porcher and C. Zaldo, *J. Alloys Comp.* **2001**, *323***,** 321

[16] M.C. Pujol, C. Cascales, M.Aguiló and F. Díaz, *J. Phys.: Condens. Matter,* 2008, *20*, 345210.

[17] A. Méndez Blas, V. Volkov, C. Cascales and C. Zaldo, *J. Alloys Comp*, **2001**, *323*, 315.

[18] M. Rico, V. Volkov, C. Cascales, E. Zaldo, *Chem. Phys.* **2002,** *279*, 73.

[19] A. Méndez-Blas, M. Rico, V. Volkov, C. Zaldo and C. Cascales, *Mol. Phys.* 2003,*101*, 941.

[20] A. Méndez-Blas, M. Rico, V. Volkov, C. Cascales, C. Zaldo, C. Coya, A. Kling and L.C. Alves, *J. Phys.: Condensed Matter* **2004***, 16*, 2139.

[21] A. Méndez-Blas, M. Rico, V. Volkov, C. Zaldo and C. Cascales, *Phys. Rev. B*, **2007**, *75***,** 174208.

[22] A. A. Kaminskii, L*aser & Photon. Rev*. **2007**, *1*, 93.

[23] A. Krueger, and F. Philippe, *Photonics Spectra,* **2004,** *38*, 46.

[24] E. Hellstrom, S. Bjurshagen, V. Pasiskevicius, J. Liu, V. Petrov, and U. Griebner, *Appl. Phys. B,* **2006**, *83*, 235.

[25] F. Brunner, T. Südmeyer, E. Innerhofer, F. Morier-Genoud, R. Paschotta, V. E. Kisel, V. G. Scherbitsky, N. V. Kuleshov, J. Gao, K. Contag, A. Giesen, and U. Keller, *Opt. Lett.*, **2002**, *27*, 1162.

[26] V. Petrov, M.C, Pujol, X. Mateos, O. Silvestre, S. Rivier, M. Aguiló, R. M. Solé, J. Liu, U. Griebner and F. Díaz, *Laser & Photon. Rev.* **2007**, *1,* 179.

[27] C. Cascales, A. Méndez-Blas, M. Rico, V. Volkov, and C. Zaldo, *Opt. Mater.* **2005***, 27*, 1672.

[28] C. Cascales M. D. Serrano, F. Esteban-Betegon, C. Zaldo, R. Peters, J. Johannsen, M. Mond, K. Peterman, G. Huber, L. Ackermann, D. Rytz, C. Dupré, M. Rico, U. Griebner, V. Petrov, *Phys. Rev. B*, **2006,** *17,* 174114.

[29] M. Rico, X. Han, J.M. Cano Torres, C. Cascales, C. Zaldo, X. Mateos, S. Rivier, U. Griebner and V. Petrov, *J. Appl. Phys,* **2008,** *103,* 083110.

[30] A. García-Cortés, X. Han, J. M. Cano-Torres, C. Cascales, C. Zaldo, X. Mateos, V. Petrov and F. J. Valle, *J. Appl. Phys*. **2007,** *101*, 063110.

[31] A. García-Cortés, J. M. Cano-Torres, M D. Serrano, C. Cascales C. Zaldo, S. Rivier, X. Mateos, U. Griebner and V. Petrov, *IEEE J. Quant. Electron.* **2007**, *43*, 758.

[32] A. Ellens, H. Andres, A. Meijerink, G. Blasse, *Phys. Rev. B* **1997,** *55,* 173. Ellens, A.; Andres, H.; M. L. ter Heerdt, H.; Wegh, R. T.; Meijerink, A.; Blasse, G. *Phys. Rev. B* **1997**, *55*, 180

[33] C. Cascales, C. Zaldo and R. Sáez Puche, *Chem. Mater.* **2005,** *17*, 2052.

[34] C. Cascales, C. Zaldo, *Chem. Mater,* **2006**, *18*, 3742.

[35] N.V. Kuleshov, A.A. Lagatsky, A.V. Podlipensky, V.P. Mikhailov and G. Huber, *Opt. Lett.* **1997**, *22*, 131

[36] M.C. Pujol, *Obtenció i caracterització de cristalls monoclinics de $KGd(WO_4)_2$ substituits amb lantànids,* Ph.D. Thesis, Universitat Rovira i Virgili, Tarragona, 2001.

[37] C. Pujol, M. Aguiló, F. Díaz, C. Zaldo, *Opt. Mater.* **1999**, *13*, 33.

[38] M. C. Pujol, M. A. Bursukova, F. Güell, X. Mateos, R. Solé, Jna. Gavaldà, M. Aguiló, J. Massons, F. Díaz, P. Klopp, U. Griebner, and V. Petrov, *Phys. Rev. B* **2002**, *65*, 165121.

[39] M.C. Pujol, R. Solé, J. Massons, J. Gavaldà, X. Solans, C. Zaldo, F. Díaz, M. Aguiló, *J. Appl. Crystallogr.* **2001,** *34*, 1.

[40] M.C. Pujol, X. Mateos, R. Solé, J. Massons, J. Gavaldà, X. Solans, F. Díaz, M. Aguiló, *J. Appl. Crystallogr.* **2002**, *35*, 108

[41] X. Han, A. García-Cortés, M D. Serrano, C. Zaldo and C. Cascales, Chem. Mater. **2007**, 19, 3002.

[42] A. García-Cortés, C. Zaldo and C. Cascales, *Opt. Mater.* **2009**, *31*, 1096.

[43] P.H. Haumesser, R. Gaumé, B. Viana E. Antic-Fidancev, and D. Vivien, *J. Phys.: Condens. Matter* **2001***, 13*, 5427.

[44] P. Porcher P, M. Couto dos Santos M and O. Malta O, *Phys. Chem. Chem. Phys*. **1999**, *1,* 397.

[45] W.T. Carnall, G.L. Goodman, K. Rajnak and R.S. Rana, *J. Chem. Phys*. **1989**, *90*, 3443.

[46] R.J. Lamminmäki, *The optical properties and simulation of the energy levels of the R^{3+} ions in rare earth oxychlorides,* Ph.D. Thesis, 1999, Annales Universitatis Turkuensis, Series A I, (Turku University Library, Finland) vol. 253.

[47] P. Porcher, Fortran routines REEL and IMAGE for simulation of d^N and f^N configurations involving real and complex crystal field parameters, **1989**, unpublished.

[48] N.C. Chang, J.B. Gruber, R.P. Leavitt, C.A. Morrison*, J. Chem. Phys.* **1982**, *76*, 3877.

[49] R.D. Shannon, P.S.Gummerman, J. Chenavas J *J. Am. Miner.* **1975,** *60*, 714.

[50] J. M. Cano-Torres, M. Rico, X. Han, M. D. Serrano, C. Cascales, C. Zaldo. F. J. Valle, V. Petrov, K. Peterman and G. Huber, to appear in *Phys. Rev. B* 2009.

[51] S. Rivier, X. Mateos, Ò. Silvestre, V. Petrov, U. Griebner, M.C. Pujol, M. Aguiló, F. Díaz, S. Vernay, and D. Rytz, *Opt. Lett.* **2007***, 33***,** 735.

[52] J. Liu, M. Rico, U. Griebner, V. Petrov, J. M. Cano-Torres, F. Esteban-Betegón, M. D. Serrano, C. Cascales and C. Zaldo, *Opt. Laser Techn.* **2007**, *39*, 558.

[53] M. Rico, J. Liu, J. M. Cano-Torres A. García-Cortés, C. Cascales, C. Zaldo, U. Griebner, V. Petrov, *Appl. Phys. B* **2005,** *81*, 621.